[PROC. OF JSCE Structural Eng. /Earthquake Eng. Vol. 2, No. 1 April 1985]

CYCLIC BENDING TESTS OF THIN-WALLED BOX BEAMS

By Yuhshi FUKUMOTO and Haruyuki KUSAMA***

This paper presents a study on the deformation behavior of thin-walled welded box beams under cyclic bending. The specimens are tested under two-point load bending to have a uniform moment occur in the central segment of the beam. Two different simple models are introduced to predict analytically the cyclic moment-curvature curves of the beams. The numerically obtained stress versus strain curves of plate elements are utilized to calculate the moment-curvature curves.

1. INTRODUCTION

For collapse study of steel structural members under extreme loading condition, such as, earthquake or wave motion, the entire behavior including cyclic loading must be considered. It is expected that a properly designed structural members would suffer damage, but would not callapse due to the ductile inelastic response under cyclic loading. The axial cyclic load-deformation behavior of steel columns has been the subject of intensive investigation in recent years. Some significant investigations in this field have recently been reported.

Popov et al.[9] and Sherman among others[10], have conducted experimental researches on inelastic cyclic behavior of steel columns and beam-columns. A considerable amount of data and some significant findings were presented. Attempts by Chen[11),12)] and Hanson[6] have also been made to develop analytical tools such as mathematical models and computed codes with which the cyclic behavior can be estimated.

When cyclic loads act on the thin-walled structural members, the plate elements are subjected to the alternating cyclic stress since the tensile and compressive force act alternatingly on the flange plate of the members. Effect of local deformation due to local instability of plate elements on the load-deformation relationship of the entire member should be an important subject to be solved.

A series of investigations has been conducted by the present authors to solve the inelastic cycli behavior of the plate elements under transverse or in-plane loading[3),4)]. The authors presented an experimental study on the inelastic cyclic load-deformation behavior of welded built-up square box short columns subjected to cyclic uniaxial loading[5]. The emphasis of the experiment was placed on the development of alternating local

* Member of JSCE, Dr. of Eng., Ph. D, Professor, Dept. of Civil Engineering, Nagoya Univ., (Chikusa-ku, Nagoya)
** Member of JSCE, Dr. of Eng., Assis. Professor, Dept. of Civil Engineering, Toyota National Tech. Coll. (2-1, Eisei-cho, Toyota-City)

instability of plate elements associated with cyclic loading sequences. The hysteretic loops of average stress versus axial strain curves for plate elements were expressed as a result.

This paper is the consecutive study of previously mentioned investigation[5] to grasp the deformation characteristics of thin-walled welded box beams under cyclic bending. Ten specimens are tested under two-point load bending to have a uniform moment occur in the central segment of the beams. Furthermore, two different simple models are introduced to predict analytically the cyclic moment-curvature curves ($M-\Phi$ curves) of the beams. The average stress versus strain relationships of plate element, which are obtained in the previous investigation, are utilized to calculate the $M-\Phi$ curves.

2. TEST PROGRAM

A total of ten square box beams were tested to obtain the load-deflection and $M-\Phi$ relationships under cyclic bending, of which, six were fabricated from SS 41 (σ_y=240 N/mm^2) mild steel (B series), the rest from HT 80 (σ_y=700 N/mm^2) high strength plates (BH series). The nominal plate thickness is 6 mm. In addition, four specimens were prepared for residual stress measurement (RES series). The measured mean yield stresses of mild and high strength steels are 348 N/mm^2 and 760 N/mm^2, respectively. A test specimen is shown in Fig. 1. Manual single fillet weld with 6 mm weld leg were used to built-up the specimens. Two intermediate diaphragms at the location right under loading points and two end diaphragms at the location rigth above supports were spot-welded to the flange and web plates.

The measured dimensions of the test specimens are listed in Table 1 with notations as shown in Fig. 1. In the B and BH series, the number following the letters (B and BH) represents the value of width-thickness

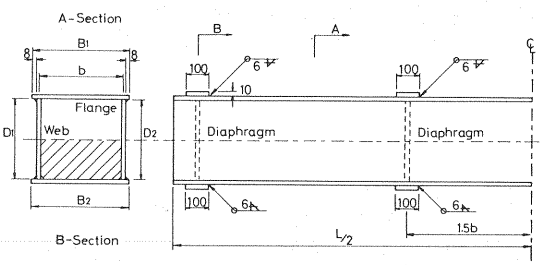

Fig. 1 Test Specimen.

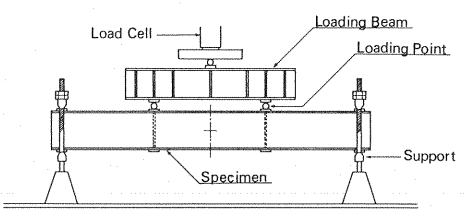

Fig. 2 Experimental Layout.

Table 1 Dimensions of Test Specimens.

Specimen	B (mm)	D (mm)	t (mm)	A (mm^2)	b/t	R	d (mm)	L (mm)	M_u (KNM)
(1)	(2)	(3)	(4)	(5)	(6)	(7)	(8)	(9)	(10)
B-40-1	263.3	234.7	5.54	5515	43.6	0.950	720	2120	144
B-40-2	263.0	235.0	5.60	5569	43.1	0.940	720	2120	153
B-60-1	383.3	354.7	5.68	8375	63.7	1.309	1080	3080	258
B-60-2	382.9	354.6	5.72	8427	63.1	1.300	1080	3080	265
B-80-1	503.1	474.4	5.62	10974	85.7	1.877	1440	4040	389
B-80-2	503.0	474.6	5.62	10971	85.7	1.877	1440	4040	402
BH-40-1	262.2	234.8	6.00	5958	40.0	1.236	720	2520	311
BH-40-2	262.2	234.8	5.99	5949	40.1	1.239	720	2520	311
BH-60-1	381.9	354.2	5.98	8805	60.2	1.884	1080	3280	493
BH-60-2	382.6	354.2	5.96	8780	60.5	1.918	1080	3280	529
RES-S-40	-	-	-	-	-	-	-	1340	-
RES-S-60	-	-	-	-	-	-	-	1640	-
RES-H-40	-	-	-	-	-	-	-	1160	-
RES-H-60	-	-	-	-	-	-	-	1640	-

Note: $B = (B_1 + B_2)/2$, $D = (D_1 + D_2)/2$, $t = (t_1 + t_2 + t_3 + t_4)/4$.

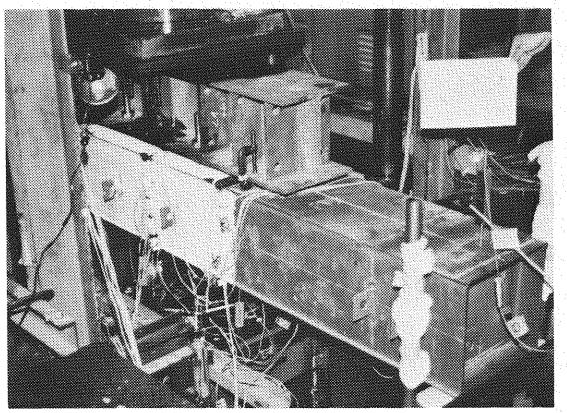

Photo 1 Test Set-Up.

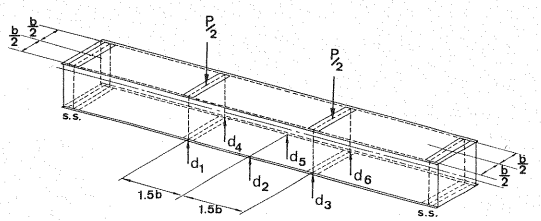

Fig. 3 Measured Points of Deflection.

ratio (b/t) of plate elements where b is the flange width between centers of webs as shown in Fig. 1. Two specimens with the same nominal dimensions are prepared for each b/t ratio. The distance between the both intermediate diaphragms is three times width, b. For the specimens of RES series, symbols S and H following the letters (RES) mean mild and high strength steels, respectively.

Ordinary two-point loading method for bending test is applied to cyclic bending test. The experimental layout to perform the cyclic bending test is illustrated in Fig. 2. The test set-up is also shown in Photo 1. The loading beam is attached by bolts to the upper pressure plate of testing machine which is fixed so as to be held in the horizontal position. Load is transmitted to the specimen through the two loading points of round steel so that the uniform bending moment occurs in the part between the both intermediate diaphragms. Both end supports are covered with teflon sheets to make the friction very low as possible. In setting the specimen, special attention is paid to coincide the geometric centroidal axis of specimen with one of loading beam to prevent twisting.

Load-control technique is employed in the initial range of loading and displacement-control technique in the neighbourhood of the peak load, P_{max}. It is defined as the reversed point that a specified increase of the center deflection of specimen from the peak load is recognized. Load-control technique is again used in the unloading state. After the load is vanished, the hydraulic ram is raised up and the specimen is turned one-half revolution round the longitudinal axis. This process is repeated seven times and, as a result, the three and half cyclic loops can be obtained experimentally.

The measured points of deflection are shown in Fig. 3 with arrows. Each measured value is represented by symbol d_i (i=1 to 6). The strains at the center of specimen are measured for all the plate elements.

Tensile Coupon Test

The test specimens are made from seven original plates, of which, three are SS 41 steel and the rest

Table 2 Tension Coupon Test Results

Specimen Series	Cross Section Area (mm^2)	Young's Modulus E ($\times 10^5 N/mm^2$)	Yield Stress σ_y (N/mm^2)	Ultimate Stress σ_u (N/mm^2)	Strain Hardening Modulus E_{st} ($\times 10^3 N/mm^2$)	Poisson's Ratio ν	Elongation %
(1)	(2)	(3)	(4)	(5)	(6)	(7)	(8)
A	220	2.08	351	461	2.21	0.247	29.1
B	229	2.09	340	443	2.24	0.251	34.7
C	221	2.11	352	446	2.31	0.238	28.6
D	237	2.13	780	849	1.37	0.228	10.9
E	235	2.13	723	792	1.29	0.223	9.8
F	232	2.12	736	811	1.85	0.224	11.0
G	234	2.12	740	805	1.57	0.228	8.8

Note: Series A for B-80-1,B-80-2;
Series B for B-60-1,B-60-2;
Series C for B-40-1,B-40-2,RES-S-40,RES-S-60;
Series D for BH-40-1,BH-40-2;
Series E for BH-60-1;
Series F for BH-60-2;
Series G for RES-H-40,RES-H-60.

Table 3 Measured Compressive Residual Stress.

Specimen (1)	b/t (2)	σ_{rc}/σ_y (3)	σ_{rc} (N/mm^2) (4)
RES-S-40	40	0.228	80.3
RES-S-60	60	0.196	69.0
RES-H-40	40	0.110	81.4
RES-H-60	60	0.076	56.2

HT 80, by flame cutting. Three tensile coupons are cut out from each original plate. Two plastic gages parallel to the tensile direction and a same gage perpendicular to the two gages are pasted on both sides of the coupon to perform the tensile coupon test. Mechanical properties of steels which are the mean of three tensile coupon test results are listed in Table 2 for each test series.

Residual Stress Measurement

Residual stresses are measured by the sectioning method with a contact-gage of 100 mm gage length. Measured residual stress patterns are all similar in shape, i. e., nearly constant compressive stresses are observed over the central portion of each plate element, and high tensile stresses are measured near the flange-web junctions. The average compressive residual rsresses over the central portion of plates are listed in Table 3.

Initial Out-of-Flatness

The welded square box beams are built-up from four plate elements. Initial out-of-deflections of only flange plate elements are measured in the three dimensional space between both intermediate diaphragms. The out-of-flatness is defined as the maximum offset from the line perpendicular to the flange-web junction line of the plate element. The average values are found to be $b/309$ and $b/552$ for SS 41 and HT 80 specimens, respectively.

3. CYCLIC LOADING TEST RESULTS

The cyclic curves of load versus center deflection of the typical beams are shown in Figs. 4 (a) ~4 (c). In these figures, the magnitude of load, P, is taken as the ordinate and the average center deflection, $\delta=(d_2+d_5)/2$, of the beam as the abscissa. Note that the load and center deflection are assumed positive when the upper flange plate is in compression at the first setting. The process of loading and unloading is carried out in a half cycle of loading. After the first half cycle is finished, all the data are registered in the measuring instrument. When the second half cycle is commenced, the final data of the first half cycle are set as the initial data of the second half cycle.

Similar procedure is repeated seven times and, as a result, three and half cyclic loops can be established. The peak bending moment of virgin curve, M_u, are given in Table 1. In Figs. 4 (a) ~4 (c), the dashed line, which represents the linear relationship, is expressed by the following equation.

$$\delta_t=Pl^3\alpha(3-4\alpha^2)/48EI+P\alpha\kappa/2GA \quad (1)$$

in which l=the distance between both end supports, I=moment of inertia, $\alpha=a/l$, a=the distance between support and loading points, G=modulus of elasticity in shear and κ=the coefficient determined by the cross sectional shape.

Ordinarily, the curve of bending moment versus curvature of section ($M-\Phi$ curve) is employed to investigate the deformation behavior of beams. $M-\Phi$ curves corresponding to Figs. 4 (a) ~4 (c) are drawn in Figs. 5 (a) ~5 (c). In these figures, the moment nondimensionalized by the yield moment is taken as the ordinate and the curvature nondimensionalized by the yield curvature as the abscissa. M and M_y are defined by the following equations.

$$M=Pa/2 \quad (2)$$

$$M_y=2I\sigma_y/(D+2t) \quad (3)$$

The curvature Φ is calculated from the deflection readings by the following equation.

$$\Phi=(\delta_l-2\delta_c+\delta_r)/l_a^2 \quad (4)$$

in which $\delta_l=(d_1+d_4)/2$, $\delta_c=(d_2+d_5)/2$, $\delta_r=(d_3+d_6)/2$ and $l_a=1.5b$.

The yield curvature Φ_y is calculated from the following equation.

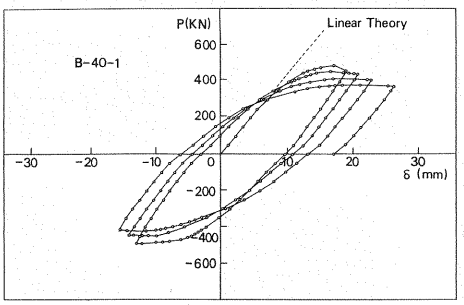

(a)

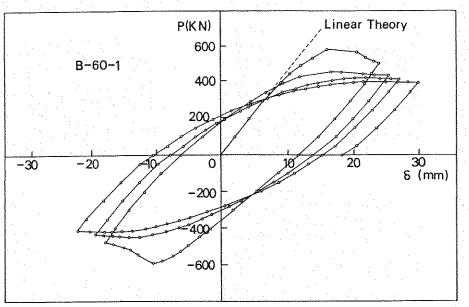

(b)

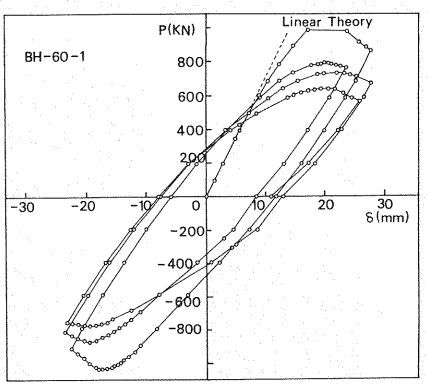

(c)

Fig. 4 Cyclic Load-Deflection Curves.

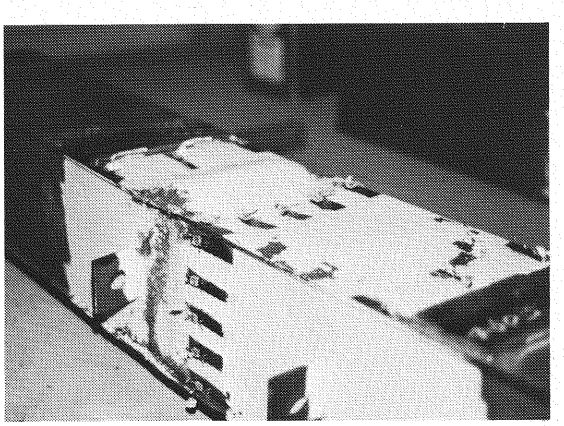

Photo 2 Specimen after Testing (B-40-2).

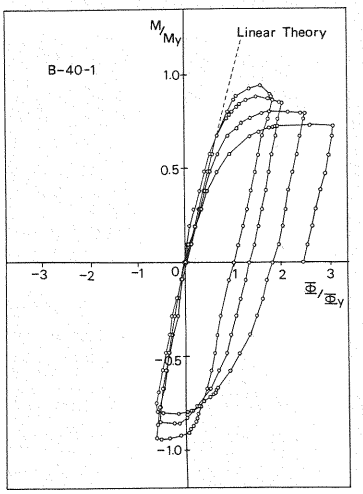

(a)

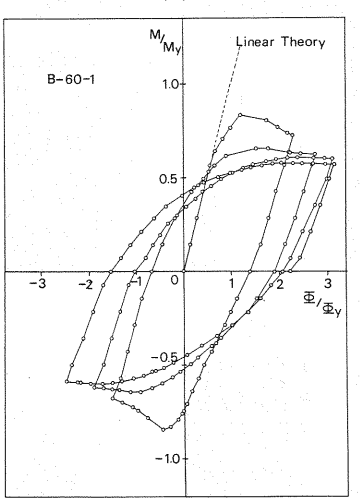

(b)

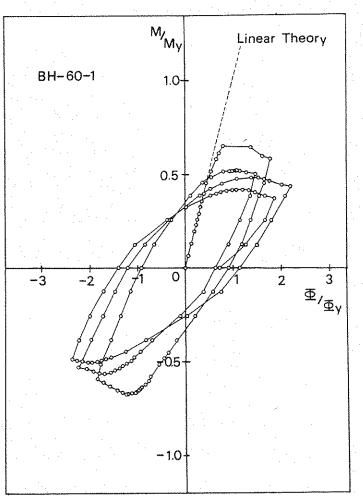

(c)

Fig. 5 Cyclic Moment-Curvature Curves.

$$\Phi_y=2(\delta_{sy}-\delta_{cy})/l_d^2 \quad (5)$$

δ_{cy} and δ_{sy} are defined by the following equations.

$$\delta_{cy}=P_y l^3\alpha(3-4\alpha^2)/48EI \quad (6)$$

$$\delta_{sy}=P_y l^3\alpha(3-4\alpha)/12EI \quad (7)$$

in which $P_y=2M_y/\alpha$.

The dashed lines denote the linear relationship of $M/M_y=\Phi/\Phi_y$.

The following findings are apparent from Figs. 4 and 5.

(1) Cyclic loops form almost always the symmetric spindle shape.

(2) The peak load and beam stiffness in each cycle are reduced as cycle increases.

(3) The gap of peak loads between the first and second cycles is drastic for the specimen with large b/t ratio. This is due to the early occurrence of local instability of flange elements.

The specimen B-40-2 after failure is shown in Photo 2, in which the out-of-plane deformation of the flange element can be recognized. The failure patterns of flange and web plate elements after cycles can be characterized by the occurrence of the highly localized deformation of a whole section. The out-of-deformation like the bellows of accordion of web element which was led by the alternate flange instability under cyclic bending may be accumulated locally after each cycle, and the beam is shortened gradually. The amount of shortening Δl=9.1 mm for BH-60-2 and Δl=8.4 mm for B-80-1, for example, are measured after test.

4. ANALYTICAL MODELS FOR CYCLIC CURVES

Two previous investigations[4),5)] by the authors are applied to calculate numerically the cyclic $M-\Phi$ curves of thin-walled beams. The object of the experiment[5)] was to obtain the out-of-plane deformation of plate element under cyclic uniaxial loading. The cyclic curves of average stress versus average strain ($\bar{\sigma}/\sigma_y-\varepsilon/\varepsilon_y$) were obtained experimentally. For example, the cyclic $\bar{\sigma}/\sigma_y-\varepsilon/\varepsilon_y$ curves of the plate elements with R=0.867 and 1.965 are shown in Figs. 6(a) and 6(b), respectively, by the solid lines. R, called buckling parameter, is defined by the following formula.

$$R=(b/t)\sqrt{12(1-\nu^2)\sigma_y/\pi^2kE} \quad (8)$$

in which k=4 is the buckling coefficient for simply supported plate with the plate aspect ratio larger than 1.0. R=0.867 and 1.965 are the minimum and maximum values of buckling parameter of the plate element in the previous investigation, respectively.

The method presented in Ref. 4) was developed for inclusion of the effect of initial deflection but not for residual stresses for the numerical calculation of cyclic behavior. Reduction of the ultimate plate strength due to the effect of residual stresses has been clarified numerically[2),7)] and its numerical effect to the ultimate strength will be included as follows in this section.

The technique, that the computed $\bar{\sigma}-\varepsilon$ curves with the measured mechanical properties and initial deflections are nondimensionalized by the modified yield stresses and strains, is herein employed. Senior author established a numerical data base from which the existing plate data of ultimate strength tests are arranged statistically[2)]. In Ref. 2), the following mean ultimate strength formulae are proposed from the results of 383 plate tests with residual stresses and 172 plate tests without residual stresses, respectively.

$$\sigma_{ul}/\sigma_y=0.968/R-0.286/R^2+0.0338/R^3,\quad 0.571\leqq R<2.0 \quad (9)$$

$$\sigma_{ul}/\sigma_y=1.133/R-0.384/R^2+0.0463/R^3,\quad 0.652\leqq R<2.0 \quad (10)$$

The difference between both Eqs. (9) and (10) denotes the reduction of plate strength due to the residual stress. Calculating the difference between both equations,

$$f(R)=0.165/R-0.098/R^2+0.013/R^3 \quad (11)$$

For example, the values of $f(R)$ corresponding to R=0.9, 1.4 and 1.9 are 0.080, 0.072 and 0.062, respectively. The change of $f(R)$ is comparatively insensitive with R. In Ref. 7), Komatsu et al. perform

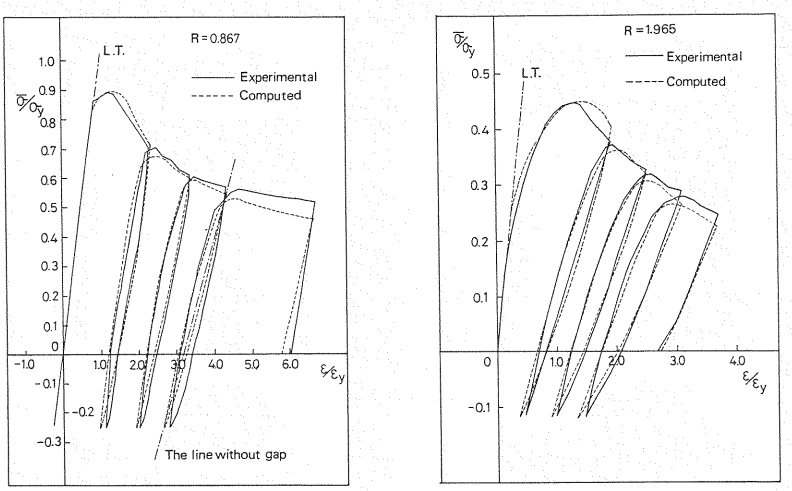

Fig. 6 Comparison of Experimental and Computed $\bar{\sigma}/\sigma_y-\varepsilon/\varepsilon_y$ curves of plate elements.

a parametric study and proposed an ultimate strength formula. They presented the similar consideration for the reduction of ultimate strength due to the residual stress. Therefore, after the cyclic $\bar{\sigma}-\varepsilon$ curves of plate elements are computed for without residual stresses, the values of $\bar{\sigma}$ and ε are nondimensionalized by the yield stress and strain modified with the value calculated by Eq. (11). The dashed lines in Figs. 6(a) and 6(b) denote the numerically analyzed results for $R=0.867$ and 1.965 to compare with the experimental curves. As seen from Figs. 6(a) and (b), the analytical results agree well with the experimental ones in the experimental range.

The maximum tension load of cyclic uniaxial loading test was fixed to be $P_{tm}=441$ kN because of the limitation of tension capacity of testing machine[5]. When the cyclic $M-\Phi$ curves of thin-walled beams are calculated, the cyclic $\bar{\sigma}/\sigma_y-\varepsilon/\varepsilon_y$ curves obtained by the cyclic uniaxial loading test are utilized as the $\bar{\sigma}/\sigma_y-\varepsilon/\varepsilon_y$ relationship of the flange elements. The numerically obtained $\bar{\sigma}/\sigma_y-\varepsilon/\varepsilon_y$ curves of thin plate under uniaxial cyclic loading are used for the calculation of the $M-\Phi$ curves to extend the limited tension range in the test. The following models, i.e., Models I and II are introduced herein to calculate $M-\Phi$ curves of the beam section.

Model I

Model I is a double-flange section model, also well known as lattice column or van der Neut-column[8], which has been frequently used to analyze the buckling strength of steel members such as box section columns. A double-flange cross section is constituted by two load-carrying flange plates and two unspecified fictitious web plates which simply serve to maintain the structural integrity of the beam. The flanges are therefore assumed to be simply supported along the longitudinal edges.

The following assumptions are used to analyze the cyclic $M-\Phi$ curves of thin-walled beams for Model I.

(1) Both upper and lower flange plate elements are connected by the double web plate elements of zero area.

(2) The cyclic $\bar{\sigma}/\sigma_y-\varepsilon/\varepsilon_y$ curves of plates under uniaxial in-plane loading are calculated by the method presented in Ref. 4).

The nondimensionalized $M-\Phi$ curves of Model I, M_1/M_{1y} and Φ_1/Φ_{1y}, are defined by the following equations.

$$M_1/M_{1y}=(\bar{\sigma}_u/\sigma_y-\bar{\sigma}_l/\sigma_y)/2 \quad \cdots\cdots (12)$$

$$\Phi_1/\Phi_{1y}=(\varepsilon_u/\varepsilon_y-\varepsilon_l/\varepsilon_y)/2 \quad \cdots\cdots (13)$$

in which $\bar{\sigma}_u(\bar{\sigma}_l)$ and $\varepsilon_u(\varepsilon_l)$ are the average stress and strain in the upper (lower) flange, respectively and they are positive in compression, and

$$M_{Iy}=Bt\sigma_y(D+t) \quad (14)$$

$$\Phi_{Iy}=2\varepsilon_y/(D+t) \quad (15)$$

Model II

Model II is a cross sectional model which includes the contribution of webs as well as double flanges for the cyclic ultimate bending strength of box beams. The following assumptions with the assumption (2) for Model I are used for the numerical analysis of $M-\Phi$ curves.

(1) Web elements are elastic and no buckling occurs during cyclic loading.

(2) The neutral axis of the beam is determined to satisfy the equilibrium condition so that the summation of normal stresses is zero in the cross section, i.e.,

$$\int_A \sigma dA=0 \quad (16)$$

Fig. 7 shows a thin-walled beam section with longitudinal strain distribution in a loading state. The linear strain distribution of the webs is assumed from assumption (1) with no stress shedding in the webs. In the figures, y_u and y_l are the distance from the obtained neutral axis of the beam to the middle surface of upper and lower flanges, respectively, $d_u=y_u-t/2$ and $d_l=y_l-t/2$. $\bar{\sigma}_u$, $\bar{\sigma}_l$, ε_u and ε_l are the same definitions for Model I. The following quadratic equation with respect to $\varepsilon_l/\varepsilon_y$ is derived using the second assumption.

$$\left(\frac{E_l}{E}+\beta\right)\left(\frac{\varepsilon_l}{\varepsilon_y}\right)^2+\frac{\varepsilon_u}{\varepsilon_y}\left(\frac{E_l}{E}-\frac{E_u}{E}\right)\frac{\varepsilon_l}{\varepsilon_y}-(1+\beta)\left(\frac{\varepsilon_u}{\varepsilon_y}\right)^2=0 \quad (17)$$

in which $\beta=D/B$, $E_u=\bar{\sigma}_u/\varepsilon_u$ and $E_l=\bar{\sigma}_l/\varepsilon_l$. When the lower flange is in the linear elastic state ($E_l/E=1$), $\varepsilon_l/\varepsilon_y$ is obtained by assuming $\varepsilon_u/\varepsilon_y$ and E_u/E of Eq. (17) and the location of the neutral axis is easily determined. When the lower flange is in the nonlinear state, the location of the neutral axis is obtained by the iteration method.

The stress hysteresis of upper and lower flanges during loading are shown schmatically in Figs. 8 (a) and (b), respectively. These curves, $\bar{\sigma}_u/\sigma_y=f_u(\varepsilon_u/\varepsilon_y)$ and $\bar{\sigma}_l/\sigma_y=f_l(\varepsilon_l/\varepsilon_y)$, are neccessary as basic informations to proceed the iterative computation. When the both curves pass the points (p_1, p_2, $\cdots$, p_i) as $0\rightarrow p_1\rightarrow p_2\rightarrow p_3\rightarrow p_4\rightarrow p_{i-1}\rightarrow p_i$, for example, we will consider the state at the i-th point. It is impossible to calculate directly $(E_l/E)_i$ and $(\varepsilon_l/\varepsilon_y)_i$ for specified $(E_u/E)_i$ and $(\varepsilon_u/\varepsilon_y)_i$ values by Eq. (17). Therefore, $(E_l/E)_{i-1}$ is used instead of $(E_l/E)_i$ as a first trial for further iteration. Thus, Eq. (17) is rewritten as follows for a first trial.

$$\left\{\left(\frac{E_l}{E}\right)_{i-1}+\beta\right\}\left(\frac{\varepsilon_l}{\varepsilon_y}\right)_i^2+\left(\frac{\varepsilon_u}{\varepsilon_y}\right)_i\left\{\left(\frac{E_l}{E}\right)_{i-1}-\left(\frac{E_u}{E}\right)_i\right\}\left(\frac{\varepsilon_l}{\varepsilon_y}\right)_i-(1+\beta)\left(\frac{\varepsilon_u}{\varepsilon_y}\right)_i^2=0 \quad (18)$$

$(\varepsilon_l/\varepsilon_y)_i$ is calculated by Eq. (18), and the second approximate of $(E_l/E)_i$ is obtained by substituting $(\varepsilon_l/\varepsilon_y)_i$ into the function $f_l(\varepsilon_l/\varepsilon_y)$. Similar procedures are repeated until the approximate of $(E_l/E)_i$ converges the value with the required accuracy.

The bending moment of Model II, M_{II}, is thus

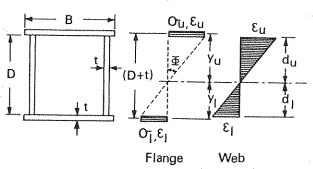

Fig. 7 Strain Distribution assumed for Model II of Thin-Walled Beams.

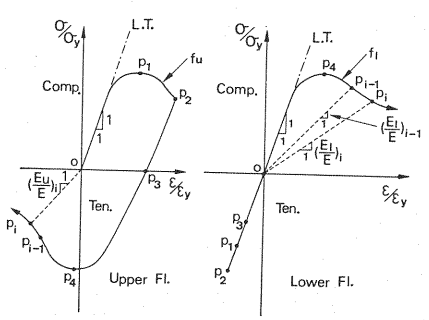

Fig. 8 Schematic Stress Hysteresis of Upper and Lower Flanges of Model II during Cyclic Loading.

calculated from the following equation.

$$M_{II}=Bt(\bar{\sigma}_u y_u-\bar{\sigma}_l y_l)+Et(\varepsilon_u d_u^2-\varepsilon_l d_l^2)/3 \quad \cdots\cdots (19)$$

The yield moment, M_{IIy}, and the nondimensionalized curvature, Φ_{II}/Φ_{IIy}, of Model II are obtained by the same formulae with Eqs. (3) and (13), respectively. Model II is simple and accurate for the computation of cyclic $M-\Phi$ curve owing to the first assumption.

The validity of the present models, Model I and Model II, is examined by comparing with other existing models for the peak strength under monotonically increased load. The ultimate moments of the box beams obtained from the present two models and other two models[1),13)] are listed in Table 4. In Table 4, $(M_u/M_y)_{EX}$ is the authors' experimental values nondimensionalized by the yield moment M_y, and $(M_u/M_y)_{MI}$ and $(M_u/M_y)_{MII}$ are calculated values for Model I and Model II, respectively. $(M_u/M_y)_E$ is calculated by the following formula[13)] based on the effective width concept.

$$\left(\frac{M_u}{M_y}\right)_E=\frac{(2+3/\bar{\alpha})(C/R)+2+\bar{\alpha}}{4+\bar{\alpha}+3/\bar{\alpha}} \quad \cdots\cdots (20)$$

in which $\bar{\alpha}=(D+t)/b$, C=the coefficient determined by plate tests, $C=0.785$ is employed from Ref. 5) and R is given by Eq. (8). The bending moment of $(M_u/M_y)_F$, M_F, is calculated by the following formula[1)] which is proposed by Fröhlich in Ref. 1).

$$M_F=(\bar{\sigma}_u^f+\sigma_y)BtH/2+\bar{\sigma}_u^w td_u(H-d_u)+\sigma_y td_l(H-d_l) \quad \cdots\cdots (21)$$

in which $H=(D+t)$, $\bar{\sigma}_u^f$ and $\bar{\sigma}_u^w$ are the ultimate stresses of flange and web plates, respectively. The ratio of the experiment divided by the reference moments are given in the columns (7) to (10). The average values and the standard deviations are also given in the table. Model II values may be close to the experiments among others with small variations.

The cyclic $M/M_y-\Phi/\Phi_y$ curves for Model I are shown in Figs. 9(a) and 9(b) by the solid lines. The dashed lines in the figure represent the corresponding experimental curves which are already given in Figs. 5(a) and (c), respectively. Note that the the parameters M_y and M_{Iy} in the ordinate in Figs. 9 denote the actual yield moment of the specimen and the modified yield moment of Model I, respectively. As seen in Figs. 9(a) and (b), the analytical curves based on Model I agree quite well with the experimental one for the beam with small b/t ratio, but the large discrepancy between the analytical and experimental curves with large b/t ratio is recognized with the number of cycles. For large b/t ratio, the flange instability occurs at an early stage of bending, and the contribution of the flange elements to the bending strength of the box beam may be reduced with as cycles increase. Instead, the behavior of web elements may become significant large for the beam strength.

Table 4 Comparison of Experimental and Several Approximate Ultimate Strengths.

Specimen	Experimental	Approximate				Experimental/Approximate			
	$(\frac{M_u}{M_y})_{EX}$	$(\frac{M_u}{M_y})_{MI}$	$(\frac{M_u}{M_y})_E$ *	$(\frac{M_u}{M_y})_F$ **	$(\frac{M_u}{M_y})_{MII}$	(A)/(B)	(A)/(C)	(A)/(D)	(A)/(E)
	(A)	(B)	(C)	(D)	(E)				
(1)	(2)	(3)	(4)	(5)	(6)	(7)	(8)	(9)	(10)
B-40-1	0.938	0.899	0.891	1.016	0.935	1.043	1.053	0.923	1.003
B-40-2	0.976	0.927	0.897	1.012	0.946	1.053	1.088	0.964	1.032
B-60-1	0.760	0.604	0.750	0.784	0.767	1.258	1.013	0.969	0.991
B-60-2	0.773	0.615	0.752	0.788	0.771	1.257	1.028	0.981	1.003
B-80-1	0.635	0.440	0.636	0.625	0.678	1.443	0.998	1.016	0.937
B-80-2	0.651	0.447	0.636	0.621	0.678	1.456	1.024	1.048	0.960
BH-40-1	0.841	0.640	0.772	0.801	0.782	1.314	1.089	1.050	1.075
BH-40-2	0.841	0.638	0.771	0.799	0.780	1.318	1.091	1.052	1.078
BH-60-1	0.647	0.448	0.635	0.614	0.664	1.444	1.019	1.054	0.974
BH-60-2	0.685	0.466	0.631	0.608	0.696	1.470	1.089	1.127	0.984
			Mean Value			1.306	1.049	1.018	1.004
			Standard Deviation			0.150	0.035	0.057	0.044

* Usami

** Fröhlich

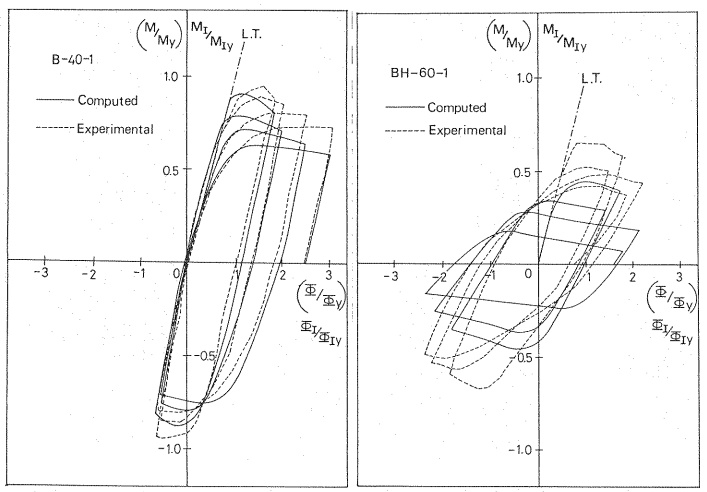

(a) (b)

Fig. 9 Comparison of Experimental and Analytical $M-\Phi$ Curves for Model I.

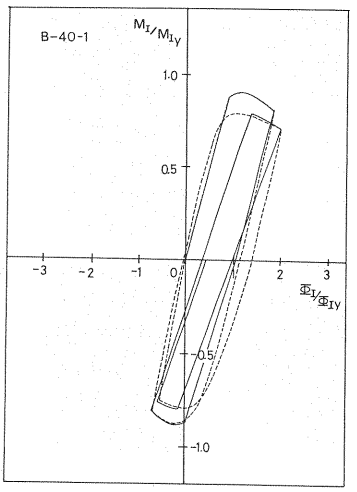

Fig. 10 Large Discrepancy of $M-\Phi$ Curves due to the Gap of $\bar{\sigma}-\varepsilon$ Relationship.

As seen from Figs. 6(a) and (b), there exists a gap between unloading and reloading paths in the cyclic $\bar{\sigma}/\sigma_y-\varepsilon/\varepsilon_y$ curves for the cyclic uniaxial loading. The physical meaning of the gap may by explained that a plate element is in a nonlinear behavior as soon as the plate is in unloading and reloading stages. When the gap between the unloading and reloading paths is neglected and a straight line is assumed as shown by a dash-dotted line in Fig. 6(a), the cyclic $M-\Phi$ curve as seen in Fig. 10 may be drawn by the solid line. The large difference of the shapes with (dashed line) or without (solid line) the gap is recognized in Fig. 10. Even though the specimen B-40-1 has the smallest gap because of the small b/t ratio, the large difference occurs as shown in the figure. The effect of the gap may thus become significant for beam with large b/t ratio.

The cyclic $M-\Phi$ curves with Model II are shown in Figs. 11(a) and (b) by the solid lines. The dashed lines in the figures are the experimental curves. From Figs. 11, the analytical curves based on Model II agree well with the experimental ones for the specimens both with small and large b/t ratios.

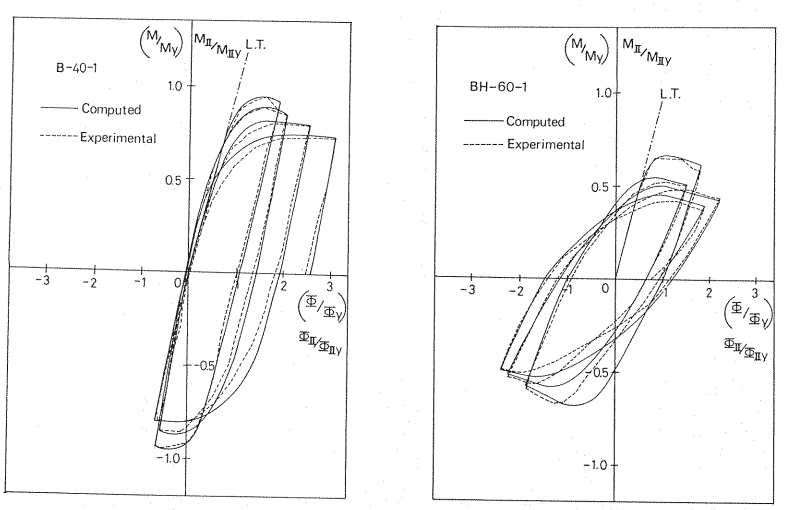

(a) (b)

Fig. 11 Comparison of Experimental and Analytical $M-\Phi$ Curves for Model II.

5. CONCUSIONS

The following main conclusions have been drawn from the present study.

(1) Cyclic loops of load versus deflection and moment versus curvature of thin-walled beams form almost always the symmetric spindle shape under cyclic bending.

(2) The ultimate strength and bending stiffness of beams become small with the number of cycles.

(3) The difference of peak loads between the first and second cycles of cyclic bending test is significant for the specimen with large b/t ratio. This is due to the early occurrence of local instability of flange elements.

(4) Two models are proposed to predict the cyclic $M-\Phi$ curves analytically. The numerically obtained cyclic $\overline{\sigma}/\sigma_y-\varepsilon/\varepsilon_y$ curves of thin plate under cyclic uniaxial in-plane loading are used for the cyclic behavior of flange elements of thin-walled beams under bending.

(5) The analytical cyclic curves based on double-flange section model (Model I) agree well with the experiment for the plate elements with small b/t ratio, but the large discrepancy between the analytical and experimental curves of the plate elements with large b/t ratio is recognized.

(6) The influence of the gap between unloading and reloading paths in the uniaxial cyclic $\overline{\sigma}/\sigma_y-\varepsilon/\varepsilon_y$ curves is significant on the cyclic $M-\Phi$ curves of thin-walled beams.

(7) The analytical curves based on Model II, in which webs are linear elastic during cyclic loading, agree quite well with the experimental ones for thinner and medium plate elements. Model II is simple and accurate enough for the cyclic bending behavior of the box beams.

6. Acknowledgment

The study presented in this paper was supported in part by the Ministry of Education, Science and Culture under Grand-in-Aid for Scientific Research.

REFERENCES

1) Fröhlich, K.-C. : Grenzträgfahigkeit von Hohlprofilen mit scharfkantiger oder ausgerundeter Eckausbilding, Technischen Universität Berlin, Dissertation, Berlin, 1983.
2) Fukumoto, Y. and Ito, Y. : Basic Compressive Strength of Steel Plates from Test Data, Proc. of JSCE, No. 344/I-1, pp. 129~139, April 1984.
3) Fukumoto, Y. and Kusama, H. : Cyclic Bending of Plates under Transverse Loading, Journal of the Engineering Mechanics Division, ASCE, Vol. 108, No. EM 3, Proc. Paper 17144, pp. 477~492, June, 1982.
4) Fukumoto, Y. and Kusama, H. : Cyclic Behavior of Plates under In-plane Loading, Engineering Structures, Jan., 1985.
5) Fukumoto, Y. and Kusama, H. : Cyclic Behaviour of Thin-Walled Box Stub-Columns and Beams, Proceedings of the Third International Colloquium on Stability of Metal Structures, Paris, pp. 211~218, Nov., 1983.
6) Higginbothan, A. B. and Hanson, R. D. : Axial Hysteretic Behavior of Steel Members, Journal of the Structural Division, ASCE, Vol. 102, No. ST 7, Proc. Paper 12245, pp. 1365~1381, July, 1976.
7) Komatsu, S. and Kitada, T. : A study of the Ultimate Strength of Compression Plate with Initial Inperfection, Proc. of JSCE, No. 270, pp. 1~14, Feb., 1978 (in Japanese).
8) Kragerup, J. : Buckling of Rectangular, Unstiffened Steel Plates in Compression, Department of Structural Engineering, Technical University of Denmark, Series R, No. 161, 1984.
9) Popov, E. P., Zayas, V. A. and Mahin, S. A. : Cyclic Inelastic Buckling of Thin Tubular Columns, Journal of the Structural Division, ASCE, Vol. 105, No. ST 11, Proc. Paper 14982, pp. 2261~2277, Nov., 1979.
10) Sherman, D. R. : Inelastic Local Buckling of Circular Tubes, US Japan Seminar on Inelastic Instability of Steel Structures and Structural Elements, Tokyo, Japan, May, 1981.
11) Toma, S. and Chen, W. F. : Analysis of Fabricated Tubular Columns, Journal of the Structural Division, ASCE, Vol. 105, No. ST 11, Proc. Paper 14994, pp. 2343~2366, Nov., 1979.
12) Toma, S. and Chen, W. F. : Cyclic Analysis of Fixed-Ended Steel Beam-Columns, Journal of the Structural Division, ASCE, Vol. 108, No. ST 6, Proc. Paper 17180, pp. 1385~1399, June, 1982.
13) Usami, T. and Fukumoto, Y. : Local and Overall Buckling Tests of Compression Members and an Analysis Based on the Effective Width Concept, Proceedings of JSCE, Vol. 326, pp. 41~50, Oct., 1982 (in Japanese).

(Received September 25 1984)